The Impact of Tropical Indian Ocean Variability on Summer Surface Air Temperature in China

KAIMING HU

Center for Monsoon System Research, Institute of Atmospheric Physics, Chinese Academy of Sciences, Beijing, and Key Laboratory of Global Change and Marine-Atmospheric Chemistry, State Oceanic Administration, Xiamen, China

GANG HUANG

State Key Laboratory of Numerical Modeling for Atmospheric Sciences and Geophysical Fluid Dynamics, and Key Laboratory of Regional Climate-Environment for East Asia, Institute of Atmospheric Physics, Chinese Academy of Sciences, Beijing, China

RONGHUI HUANG

Center for Monsoon System Research, and State Key Laboratory of Numerical Modeling for Atmospheric Sciences and Geophysical Fluid Dynamics, Institute of Atmospheric Physics, Chinese Academy of Sciences, Beijing, China

(Manuscript received 19 October 2010, in final form 29 March 2011)

ABSTRACT

Evidence is presented that the boreal summer surface air temperature over south China and northeast China is remotely influenced by the Indian Ocean Basin mode (IOBM) sea surface temperature (SST) anomalies. Above-normal temperature in south China and below-normal temperature in northeast China correspond to a simultaneous Indian Ocean Basin warming. The teleconnection from Indian Ocean SST anomalies to China summer surface air temperature is investigated using observations and an atmospheric general circulation model (AGCM). The results herein indicate that the tropical Indian Ocean Basin warming can trigger a low-level anomalous anticyclone circulation in the subtropical northwest Pacific and an anomalous cyclone circulation in midlatitude East Asia through emanating a baroclinic Kelvin wave. In south China, the reduced rainfall and downward vertical motion associated with the anomalous low-level anticyclone circulation lead to above-normal summer surface air temperature. In northeast China, by contrast, upward vertical motion associated with the anomalous cyclone leads to below-normal summer surface air temperature.

1. Introduction

High temperature extremes can cause massive deaths from hyperthermia, large-scale catastrophic crop failures, and shortages of water resources and power supplies (Haines et al. 2006; McMichael et al. 2006). Officials and the public are beginning to recognize the need for enhanced systematic mitigation actions to reduce the increasing risk of extreme heat to national economics, the environment, and society. In China, these harmful effects are most obvious for densely populated regions. Therefore, understanding the factors and the processes for interannual variation of summer surface temperature over China is of great socioeconomic importance. There have been a number of studies on the climatology and interdecadal variation in such extreme events in China (Hu 1997; Hu et al. 2003; Shi et al. 2011; Wei and Chen 2009; Zhai et al. 1999). However, the year-to-year variations of these high temperature extremes are not well understood.

The interannual variations of summer climate in China are largely controlled by the variability in the East Asia summer monsoon (Huang and Wu 1989; Huang et al. 2004). A number of studies (Yang et al. 2007; Li et al. 2008; Xie et al. 2009) reveal that the East Asia summer monsoon is affected by the interannual fluctuation of the Indian Ocean Basin sea surface temperature anomalies (SSTAs), which is referred as the Indian Ocean Basin mode (IOBM) (Klein et al. 1999; Saji et al. 1999). The mechanism for this influence is revealed by Xie et al. (2009) and is demonstrated as follows. IOBM SST warming forces a Matsuno–Gill (Matsuno 1966;

Corresponding author address: Gang Huang, LASG/IAP/CAS, P.O. Box 9804, Beijing 100029, China.
E-mail: hg@mail.iap.ac.cn

DOI: 10.1175/2011JCLI4152.1

Gill 1980) pattern in the tropospheric temperature. The warm tropospheric Kelvin wave propagates into the western Pacific, inducing Ekman divergence in the subtropical northwest Pacific (NWP) to suppress convection and develop an anticyclonic circulation near the surface. The NWP anticyclone, with weak convection, leads to the summer rainfall anomalies in East Asia. Recent forecast experiments using a coupled general circulation model (GCM) also confirm this tropical Indian Ocean (TIO) teleconnection to the NWP and East Asia summer climate (Chowdary et al. 2011). However, these studies mainly focus on summer rainfall anomalies in East Asia.

Based on the above introduction, we have the first question, whether IOBM SST anomalies in the tropical Indian Ocean may also have a significant impact on China summer surface air temperature anomalies on an interannual time scale. When SSTs are warming in the tropical Indian Ocean Basin, an anomalous low-level anticyclone would develop in the subtropical northwest Pacific, and cyclone anomalies would develop in the midlatitude East Asia through the propagating East Asia–Pacific (EAP) (Huang and Lu 1989; Huang and Yan 1999)/Pacific–Japan (PJ) (Nitta 1987) wave train. The anticyclone and cyclone may be able to affect China surface air temperature through changing the temperature advection, vertical motion, and adiabatic heating.

Meantime, the decadal change in the amplitude of interannual temperature variability also has an impact on the frequency of high temperature extremes. Our previous studies (Xie et al. 2010; Huang et al. 2010) have shown that the interannual variability of summer tropical Indian Ocean SST has become larger after the late 1970s. Thus, we have the second question, whether the interannual variability of the TIO-related summer surface air temperature in China is also increased after the late 1970s.

The main aim of this study is to investigate the above two questions by data analysis and model studies. The rest of the paper is organized as follows: Section 2 describes the data and numerical simulation. Section 3 presents the observational evidences. Section 4 diagnoses the model output. Section 5 includes a summary and some discussions.

2. Data and model

The China monthly-mean surface air temperature and precipitation dataset used in this study includes 160 stations in China for the period 1951–2008 and was provided by the China Meteorological Administration's National Climate Center.

The global precipitation dataset used in this study is the monthly-mean Climate Prediction Center (CPC) Merged Analysis of Precipitation (CMAP; Xie and Arkin 1996) for the period 1979–2008, which is available on a 2.5° × 2.5°grid.

The SST used in the present study is the Met Office Hadley Centre Sea Ice and Sea Surface Temperature version 1 (HadISST1) dataset (Rayner et al. 2003) for the period 1951–2008. This SST dataset has a resolution of 1° × 1°.

The present study uses winds, vertical velocity, and air temperature from the National Centers for Environmental Prediction–National Center for Atmospheric Research (NCEP–NCAR) (Kalnay et al. 1996) for the period 1951–2008. The monthly-mean temperature advection derived from the NCEP daily winds and temperature is also used in the present analysis. These variables are available on 2.5° × 2.5°grids.

We use the Community Atmosphere Model, version 3 (CAM3) at T42 resolution (equivalent to 2.8° latitude × 2.8° longitude) in the horizontal and 23 sigma levels in the vertical. Details of the models are provided in Collins et al. (2006). A 21-member ensemble of CAM3 simulations are performed with HadISST1 observations as surface boundary conditions over the global domain for a 51-yr period from 1950 to 2000. Each member simulation differs only in the initial conditions. We select these model simulation data from 1979 to 2000 in this study.

To be consistent with the global precipitation dataset that is available starting from 1979, our study mainly focuses on the impact of the TIO on China summer temperature anomalies during 1979–2008. Moreover, we also discuss the decadal change of the interannual variability of the TIO and China summer surface temperature during the period from 1951 to 2008. Throughout this study, the analysis is performed for interannual variations on time scales shorter than 8 yr. A linear trend has been subtracted from raw anomalies to remove decadal and longer time-scale variations. For a 30-yr time series, correlations of 0.31 and 0.37 reach the 90% and 95% confidence levels, respectively, based on the Student *t* test.

3. Observational evidence

a. The relationship between the TIO and China summer temperature

To examine the relationship between the spatial and temporal variability of the summer [June–August (JJA) mean] surface air temperature over China and the TIO SST anomalies, we first perform a singular value decomposition (SVD) analysis on the summer surface air temperature over China and simultaneous Indian Ocean

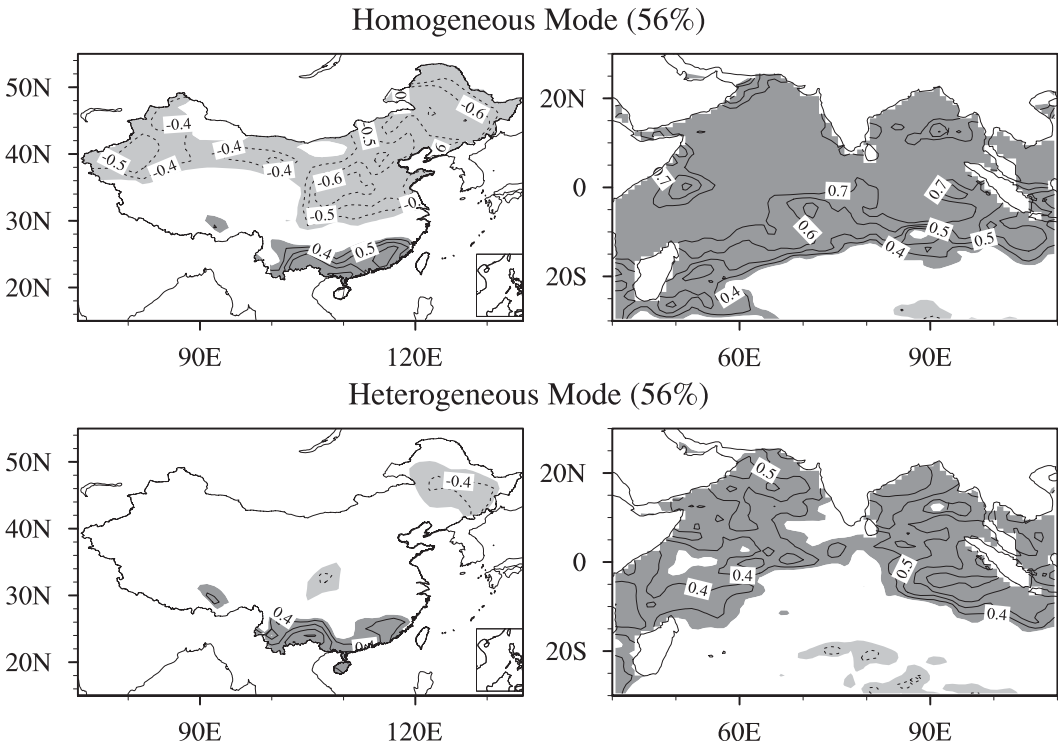

FIG. 1. First leading SVD (top) homogeneous and (bottom) heterogeneous correlation maps of JJA (right) SST over the Indian Ocean and (left) surface air temperature over China. SVD analysis is based on the data from 1979 to 2008. Contours interval is 0.1 and shades denote 90% confidence level.

SST anomalies (30°S–30°N, 30°–110°E) from 1979 to 2008 [details of the SVD method are provided on the NCAR Command Language (NCL) Web site at http://www.ncl.ucar.edu/].

As Fig. 1 shows, the first leading homogeneous SVD mode (the top panel of Fig. 1) is characterized by an IOBM SST warming and a seesaw surface temperature pattern between south and north China. When there is basinwide warming in the tropical Indian Ocean, the south China (SC) summer surface temperature is above normal and north China, especially the northeast China (NEC) surface temperature, is below normal. This mode accounts for 56% of the total squared covariance.

To confirm the relationship between the summer TIO SST anomalies and simultaneous China surface air temperature, we also calculate the heterogeneous correlation coefficient of the first leading SVD mode in the bottom panel of Fig. 1. The first heterogeneous SVD mode is also characterized by the IOBM pattern in SST anomalies and seesaw pattern in surface air temperature anomalies between south China and northeast China. Compared with the homogeneous SVD mode, the heterogeneous correlations are lower but with a similar pattern. In heterogeneous correlation map, the positive correlations of SST are mainly distributed in the tropical Indian Ocean and South China Sea, with the maximum correlation coefficient above 0.7; the negative correlations of surface air temperature are mainly distributed in northeast China, with the correlation coefficient below about −0.4 (passing the 95% confidence level); and the positive correlation coefficients of surface air temperature are distributed in south China, with the maximum correlation coefficient above 0.5 (passing the 95% confidence level).

Additionally, the second leading SVD mode shows a positive correlation between the south subtropical Indian Ocean SST anomalies and the simultaneous surface air temperature in the Yangtze River (the figure is not shown). However, the second mode only accounts for 14% of the total squared covariance. Thus, the present study will focus on the first leading SVD mode, which suggests a close relationship between IOBM SST anomalies and China surface air temperature.

To further demonstrate the relationship between the Indian Ocean SST and China surface air temperature, we use the SST averaged in the tropical Indian Ocean (20°S~20°N, 40°E~100°E) as an index of the IOBM and correlate it with China surface air temperature from 1979 to 2008. The correlation pattern shows great similarity with the first SVD mode, with a positive center in

south China and a negative center in northeast China (Fig. 2). This strongly suggests a potential link between the seesaw pattern in surface air temperature anomalies in China and the Indian Ocean SST in summer.

b. *The possible remote teleconnection from the TIO to China temperature*

High surface air temperatures are often caused by less precipitation, long-term sustaining circulation anomalies, radiation anomalies, and atmospheric downward motion. For example, the serious heat wave in Europe during 2003 due to persistent anticyclonic conditions, a lack of precipitation, radiation anomalies, downward motion, and land–air feedback from May to August (Black et al. 2004; Fischer et al. 2007). Here, we investigate the IOBM-induced summer China surface air temperature anomalies through discussing these factors in Fig. 3.

First, we discuss the role of local precipitation anomalies in the impact of the TIO on China surface air temperature. Figure 3a shows the correlation map between TS_PC1 (the time series of the first leading China summer surface air temperature SVD mode in Fig. 1) and JJA mean precipitation in East Asia during 1979–2008. Corresponding to the seesaw surface air temperature anomalies, the rainfall is below normal, with the minimum correlation coefficients around −0.6 in the southernmost part of China (the bottom rectangle in Fig. 3a) and above-normal in the western part of northeast China (the top rectangle in Fig. 3a). The lack of rainfall may contribute to warm surface air temperature anomalies in south China. Analogously, the above-normal precipitation in the western part of northeast China may contribute to local cooling. However, the correlation between TS_PC1 and precipitation is weak in the eastern part of northeast China. The precipitation anomalies may not have a substantial impact on the local surface temperature in the eastern part of northeast China.

Second, we discuss the role of vertical motion in Fig. 3c by calculating the correlation coefficient between TS_PC1 and vertical velocity at 500 hPa. As Fig. 3c shows, the downward motion controls south China and the upward motion controls northeast China when the surface air temperature is above-normal in south China and below-normal in northeast China. The upward motion anomalies at 850 hPa (figure is not shown) is the same as Fig. 3c. The result is consistent with the theory that the downward movement leads to air warming by adiabatic heating, and the upward movement can suppress such adiabatic heating. Thus, the summer surface air temperature in both south China and northeast China is influenced by vertical motion anomalies.

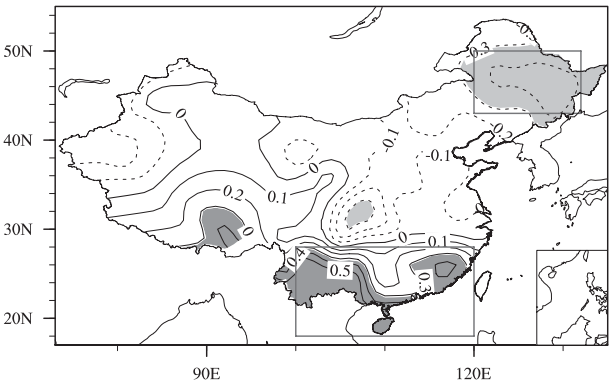

FIG. 2. Correlation of China summer surface air temperature with simultaneous IOBM index (area-average SST over 20°S–20°N, 40°–100°E) during 1979–2008. Contours interval is 0.1, and shading denotes 90% confidence level.

Third, we discuss the role of temperature horizontal advection in Fig. 3e. Since the terrain is complex in south China and since the lower-level air temperature anomalies are well coherent with surface air temperature anomalies in China (shown in Fig. 4), we calculate the correlation of TS_PC1 with the lower-level (vertical average from 1000 to 850 hPa) temperature horizontal advection anomalies instead of the temperature horizontal advection at the surface. As Fig. 3e shows, the horizontal advection correlation with TS_PC1 is weak in both south China and northeast China. The results illustrate that summer-mean temperature horizontal advection anomalies may not play an important role in the process of the impact of the TIO on summer surface air temperature in China.

The above analysis suggests that the seesaw pattern in the summer surface air temperature anomalies in China partly results from the follow factors: precipitation and vertical motion anomalies. Furthermore, the correlation maps in Figs. 3b, 3d, and 3f, which are calculated using SST_PC1 (the time series of the first leading SVD mode of the Indian Ocean SST in Fig. 1), are similar to Figs. 3a, 3c, and 3e, respectively, which suggests that the Indian Ocean basinwide SST anomalies have a potential link with these precipitation and circulation anomalies which, in turn, contribute to the summer surface air temperature anomalies in China.

The preceding four paragraphs discuss the role of the precipitation and circulation anomalies in the process of the impact of the TIO on summer surface air temperature in China. The below-normal precipitation and downward motion may lead to warmer-than-normal summer south China surface air temperature, and the upward motion may lead to cooler-than-normal summer surface temperature in northeast China. And these

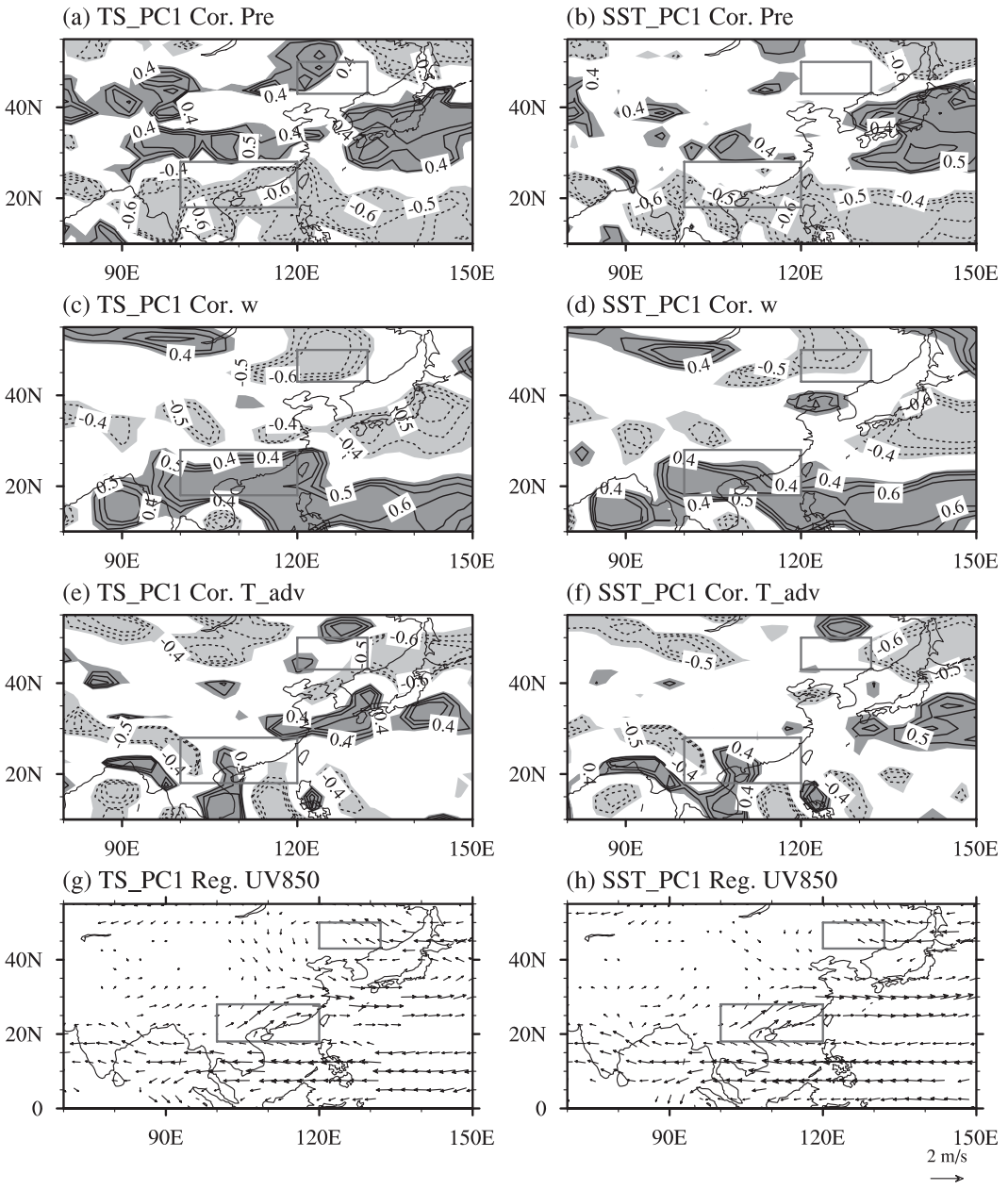

FIG. 3. Correlation of JJA (a) precipitation, (c) upward motion at 500 hPa (positive value represents subsidence), (e) lower-level (vertical average from 1000 to 850 hPa) temperature horizontal advection with TS_PC1 (of Fig. 1) and regression of JJA 850-hPa wind on TS_PC1. (right) As in (left), but using SST_PC1 (of Fig. 1). Wind vectors and shading denote 90% confidence level.

precipitation and circulation anomalies are associated with IOBM SST anomalies.

Moreover, both JJA precipitation anomalies and vertical movement anomalies show a prominent meridional dipole structure in Fig. 3. Below-normal precipitation and downward vertical motion anomalies mainly are located between the equator and 28°N. Above-normal precipitation and upward vertical motion anomalies are in the midlatitude, especially over Japan and northeast China. Meantime, an anomalous anticyclone lies over south China and the northwest Pacific and an anomalous cyclone is seen over Japan, Korea, and northeast China (Figs. 3g and 3h). The meridional dipole pattern of precipitation and vertical motion anomalies is consistent with the low-level circulation anomalies, which resemble the EAP/PJ pattern. How do

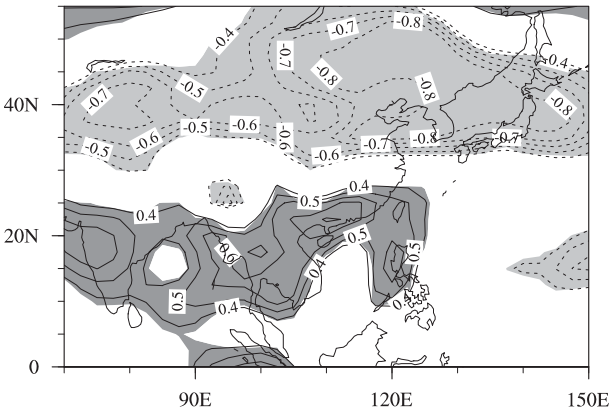

FIG. 4. Correlation of lower-level (vertical average from 1000 to 850 hPa) air temperature with the TS_PC1 (of Fig. 1) during 1979–2008. Contours interval is 0.1, and shading denotes 95% confidence level.

the SSTAs of the IOBM pattern impact the EAP/PJ-like pattern?

Previous studies (Xie et al. 2009) illustrate that IOBM pattern SSTAs can affect East Asia summer climate by a propagating Kelvin wave. To demonstrate that, we calculate the correlations of 850-hPa wind velocity and the lower-level tropospheric temperature (vertical average from 850 to 200 hPa) with the SST_PC1 and TS_PC1 during the period of 1979–2008.

As Fig. 5b shows, when the tropical Indian Ocean SSTAs display a basinwide warming pattern, the troposphere temperature displays a Matsuno–Gill pattern with the maximum correlation over the eastern TIO. A Kelvin wave wedge penetrates the western Pacific along the equator, with a pronounced anticyclonic circulation on its northern flank. A PJ/EAP-like wave train propagates to high latitude, with a low-level cyclonic circulation over north Japan, Korea, and eastern north China. Coupling with the circulation anomalies, below-normal rainfall is localized on the south side of the northwest Pacific anticyclone and above-normal rainfall on the north side of the northwest Pacific anticyclone. The precipitation, 850-hPa wind, and tropospheric temperature anomalies in Fig. 5a are similar to those in Fig. 5b. In Fig. 5a, the tropospheric temperature anomalies still resemble a Matsuno–Gill pattern, although the correlations are weaker than Fig. 5b, with the maximum correlation about 0.4 in the east Indian Ocean. Meantime, the PJ/EAP pattern is also obvious. The results are consistent with the Kelvin wave–induced Ekman divergence (WIED) mechanism of Xie et al. (2009). The AGCM results also confirm such a Kelvin WIED mechanism in section 4.

Based on the above discussions, we propose the possible mechanism for the impact of the IOBM pattern

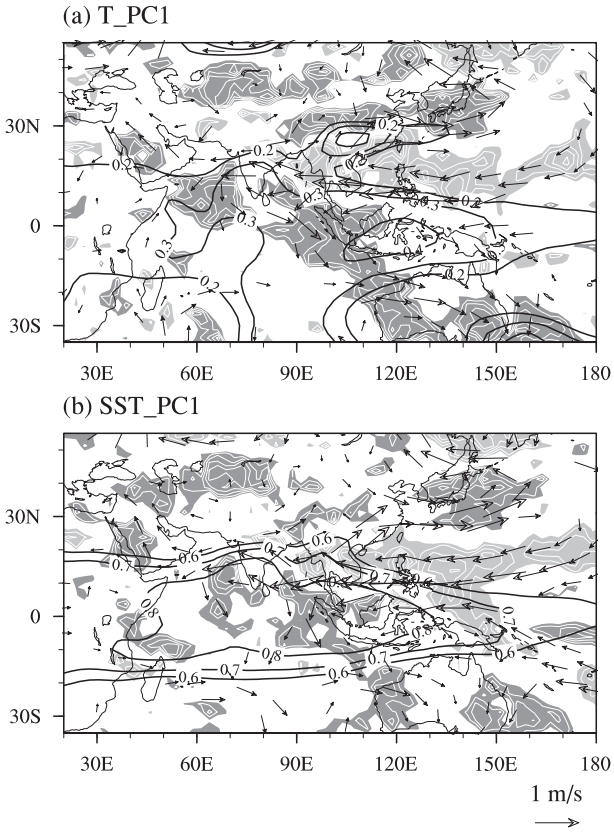

FIG. 5. Correlation with (a) TS_PC1 (of Fig. 1) and (b) SST_PC1 (of Fig. 1): summer precipitation (white contour interval is 0.1 with $|r| > 0.31$; dark shades denote positive correlation and 90% confidence level, and light shades denote negative correlation and 90% confidence level), 850-hPa wind (regression; vector), and tropospheric temperature (vertical average from 850 to 200 hPa; contours). Wind vectors denote 90% confidence level. Analysis is based on the observational data during 1979–2008.

SST anomalies on China surface temperature as follows. The IOBM SST anomalies emanate a baroclinic Kelvin wave into the Pacific. The Kelvin wave triggers suppressed convection and an anomalous anticyclone over the NWP and south China. The suppressed convection over the NWP leads to an anomalous cyclone over Japan, South Korea, and northeast China through a PJ/EAP meridional teleconnection. The meridional dipole circulation anomalies in East Asia lead to a seesaw pattern in surface air temperature anomalies in China through changing the vertical motion and rainfall patterns.

c. The decadal change of interannual variability of TIO-inducing China temperature anomalies

We have investigated the impact of IOBM SST anomalies on China summer surface air temperature during 1979–2008 in sections 3a and 3b. Our previous

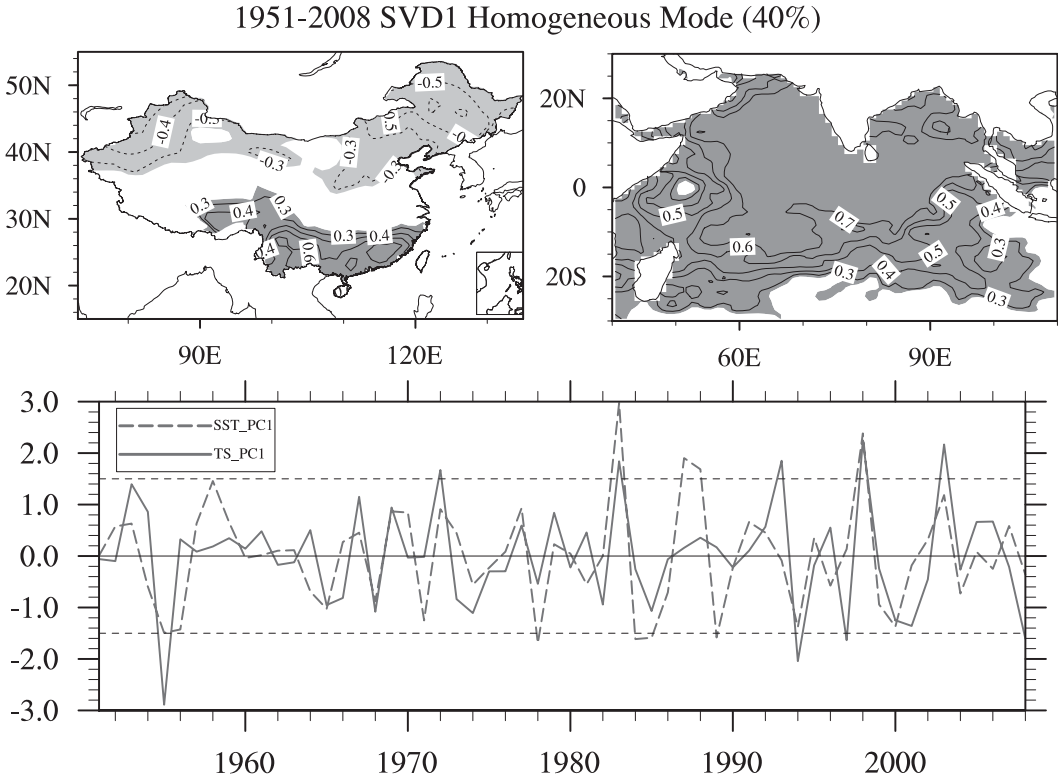

FIG. 6. (top) First leading SVD homogeneous correlation map (contours; shading denotes 90% confidence level) of summer (right) SST over the Indian Ocean and (left) surface air temperature over China. (bottom) Standardized time series of first leading SVD mode. SVD analysis is based on the data from 1951 to 2008.

studies (Xie et al. 2010; Huang et al. 2010) have shown that the interannual variability of summer tropical Indian Ocean SST has become larger after the late 1970s. The question of whether the interannual variability of TIO-related summer surface air temperature in China has also become larger will be investigated in this section.

Figure 6 shows the SVD analysis of summer TIO SST (30°S–30°N, 30°–110°E) and simultaneous China surface air temperature from 1951 to 2008, with the same domain as Fig. 1. The first leading SVD pattern is the same as Fig. 1, illustrating that the results of the SVD analysis are robust.

Although the spatial patterns are robust, the interannual variability of SST_PC1 in Fig. 6 has experienced a prominent increase in the late 1970s. A prominent increase is also seen in the interannual variability of TS_PC1 (Fig. 6). To document this decadal change, we partition the time series into pre- and postshift periods of 1951–79 and 1980–2008, respectively. During the period of 1951–79, there are only 2 and 1 yr when the absolute value of standardized TS_PC1 and SST_PC1, respectively, exceed 1.5. During the postshift period, by contrast, there are 6 and 7 yr when the absolute values of the standardized PC1 exceed 1.5 for TS_PC1 and SST_PC1, respectively. These suggest that the interannual variability of the TIO-induced China summer surface air temperature is larger during the recent decade.

Additionally, we calculate the SC index (area-mean surface air temperature in the bottom rectangle in Fig. 2) and the NEC index (area-mean surface air temperature in the top rectangle in Fig. 2) to represent the interannual variation of south China and northeast China summer surface temperatures, respectively. Figure 7 shows the standardized IOBM index, SC index, and NEC index. Consistent with previous studies, the interannual variability of the IOBM index has experienced a prominent increase in the late 1970s. We also note that the interannual variability of the NEC index has experienced an increase in the late 1970s. There are 5 yr when the absolute value of the standardized NEC index exceeds 1.5 during the postshift period but no years during the preshift period. The SC index has not experienced a significant increase during the recent decade. However, the correlation between the SC index and the IOBM index is still significant (correlation coefficient is 0.35 for 51 yr). This suggests that the Indian Ocean SST is only one of several factors that influence

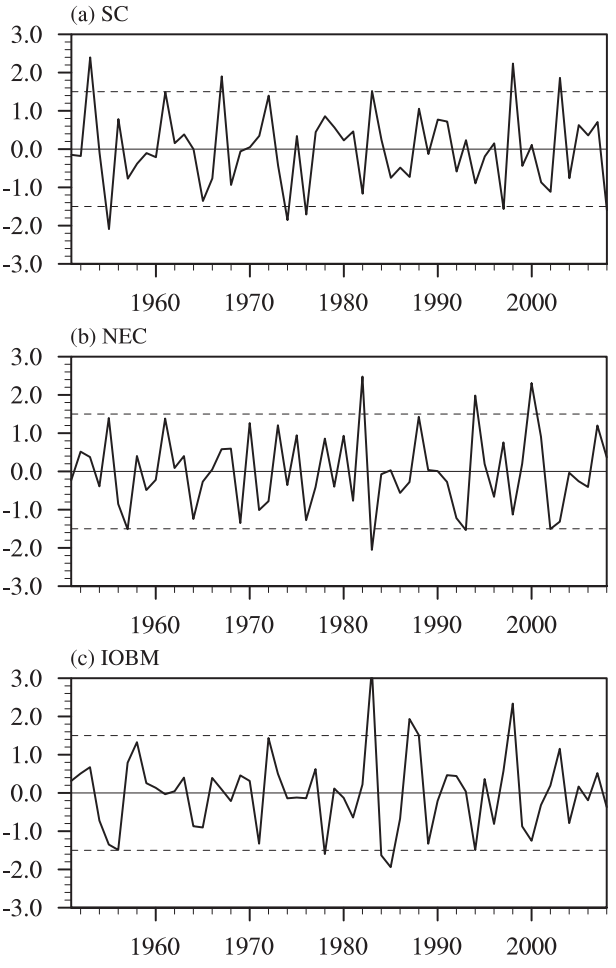

FIG. 7. Normalized time series of (a) SC index [JJA mean China surface air temperature over south China (18°–28°N, 100°–120°E)], (b) NEC index [JJA mean China surface temperature over northeast China (43°–50°N, 120°–132°E)]. Horizontal dashed line denotes 1.5 standard deviation.

south China summer surface temperature. Some other factors may influence the year-to-year variation of south China temperature. Thus, despite that the interannual variability of the TIO-induced surface air temperature in China has experienced a significant decadal change, the observed interannual variability of summer surface temperature in south China has not experienced such a decadal change.

4. Model studies

We first evaluate the model simulation skills by performing the empirical orthogonal function (EOF) analysis for the ensemble-mean variability of JJA 850-hPa wind field over East Asia (5°–60°N, 90°–150°E) during 1979–2000. Figure 8 compares the first and second leading EOF (EOF1 and EOF2, respectively) modes with observations. In the observations, the first mode explains 48.1% of the total variance, featuring an anticyclone over the northwest Pacific and a cyclone over the midlatitude associated with dipole rainfall anomalies over East Asia (Fig. 8, top left). The second mode explains 14.6% of the variance and also featuring a cyclone and an anticyclone dipole over East Asia, which shift northward when compared with the EOF1 mode. The EOF2 mode corresponds to dipole rainfall anomalies in the tropical western Pacific.

The model ensemble-mean simulation captures the salient features of the observed EOFs with the following differences: 1) the model EOF1 explains a much larger fraction of the variance, possibly because of weaker noise than in observations; 2) the observed midlatitude cyclone anomalies are not captured by the model simulation; 3) in the model EOF2, the observed midlatitude cyclone anomalies are also not captured by the model simulation; and 4) the associated precipitation anomalies are also a little different from observations. We also compare the time series of observation and model simulation EOF modes. The correlation coefficient is 0.7 and 0.39 for the first principal component (EOF-PC1) and second principal component (EOF-PC2) between observations and the model simulation during 1979–2000. The results suggest that the ensemble simulation can capture a reasonable amount of climate variation over East Asia in summer, especially in the tropical and subtropical regions. In the midlatitude and high-latitude regions, the model simulation skill is low, possibly because of the strong atmosphere internal variability in high latitudes.

Since the terrain is complex in south China, we choose lower-level (vertical average is from 1000 to 850 hPa) air temperature anomalies to indicate the interannual variability of surface air temperature in China. Indeed, as Fig. 4 shows, a close relationship exist between the lower-level temperature and surface air temperature anomalies in observations. Thus, it is reasonable to use lower-level air temperature anomalies to represent surface air temperature variation.

Figure 9 shows the SVD analysis of summer TIO (30°S~30°N, 40°E~110°E) SST and simultaneous lower-level air temperature of a 21-member ensemble mean over East Asia and the northwest Pacific (0°~55°N, 90°E~180°) during 1979–2000. The first leading SVD mode explains 80.5% of the total squared covariance between the lower-level air temperature and SST anomalies. The SST pattern displays an IOBM warming pattern with maximum correlation in the tropical Indian Ocean. The lower-level air temperature pattern is characterized by a warming belt in the tropics (from about the equator to 25°N), with an obvious warm tongue extending

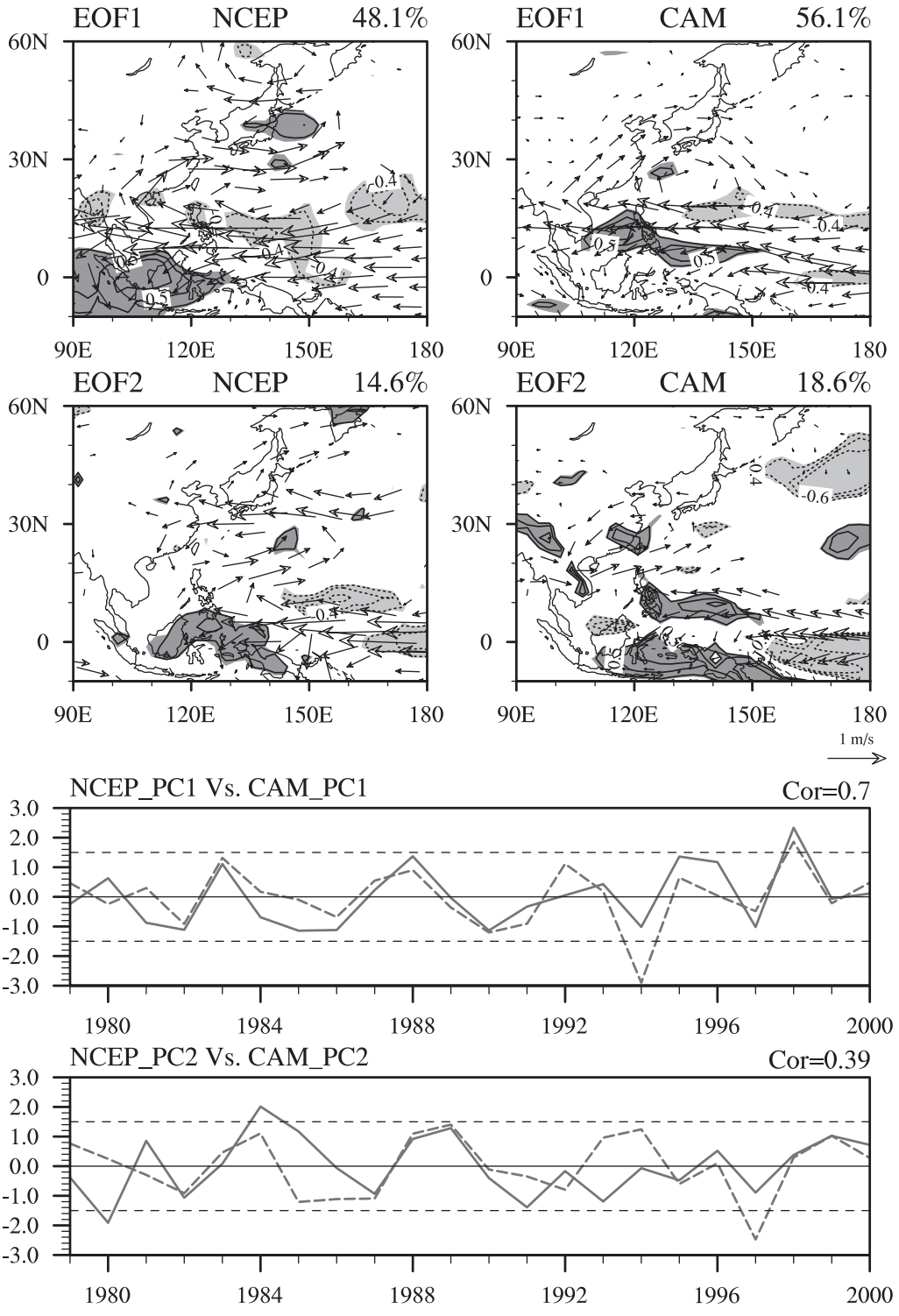

FIG. 8. (top) Correlation coefficient of JJA mean precipitation (contours; shading denotes 90% confidence level) and regression coefficient of JJA mean 850-hPa winds (vector; vectors denote 90% confidence level) with PC1 and PC2 of 850-hPa wind in (left) observation and (right) ensemble-mean simulation during the period 1979–2000. (bottom) Standardized time series of EOF1-PC and EOF2-PC of 850-hPa wind in observation (solid lines) and the ensemble-mean simulation (dashed lines). EOF analysis covers East Asia (5°–60°N, 90°–150°E) during the period of 1979–2000. EOF1 (EOF2) pattern of observation and ensemble-mean simulation account for 48.1% (14.6%) and 56.1% (18.6%) of their total variance, respectively. Correlation coefficient is 0.70 and 0.39 for EOF-PC1 and EOF-PC2, respectively, between observation and ensemble-mean simulation.

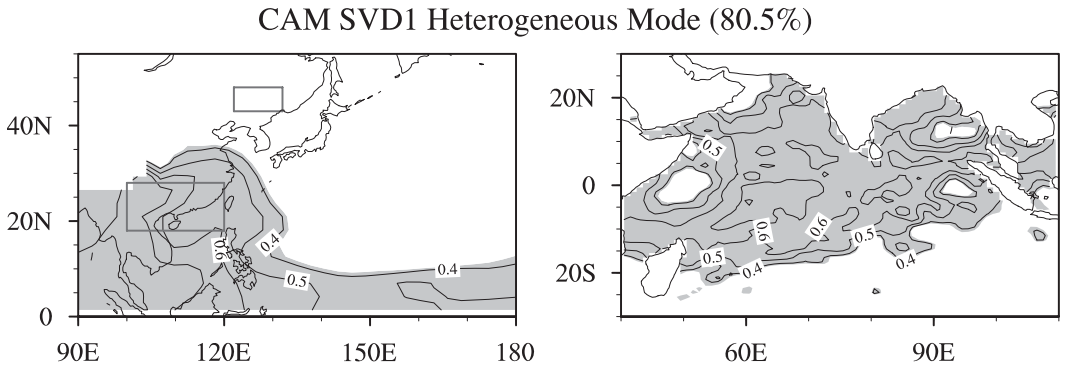

FIG. 9. First leading SVD heterogeneous correlation map of (right) summer SST over the Indian Ocean (contours) and (left) 21-member ensemble-mean simulation lower-level (vertical average from 1000 to 850 hPa) air temperature (contour). SVD analysis is based on the data from 1979 to 2000. Shading denotes 90% confidence level.

northeastward into south China and a weak cold center into the North Pacific (about 30°~40°N, 150°E~180°).

To further demonstrate the relationship between the IOBM SST anomalies and East Asia lower-level air temperature in the ensemble-mean simulation, we calculate the correlation of the IOBM index with the ensemble-mean simulation lower-level (vertical average from 1000 to 850 hPa) air temperature over East Asia and the North Pacific in Fig. 10. The correlation pattern is the same as the first SVD pattern, displaying a warm tongue (correlation coefficient above about 0.5) in south China and a cold center in the North Pacific.

Since the relationship between the surface air temperature and lower-level air temperature is close, the warm tongue in the lower-level troposphere in south China means that the surface air temperature is above normal when the Indian Ocean SST is warmer than normal, which is consistent with the observational analysis in section 3. But we note that the negative correlation center in the midlatitude is weak and does not extend westward to northeast China, which is possibly related to the low simulation skill of the AGCM in the midlatitude (Fig. 8).

Corresponding to the IOBM SST warming pattern, the circulation anomalies at 850 hPa display an anomalous anticyclone over the subtropical northwest Pacific and south China but no significant anomalous cyclone circulation in the midlatitude. The circulation anomalies are consistent with the lower-level air temperature anomalies, which are significant in the subtropical region but weak in northeast China.

To test the teleconnection mechanism from the TIO to summer surface air temperature in China, we calculate the correlation of the 21-member ensemble-mean precipitation and tropospheric temperature (850–200-hPa vertical averages) with the time series of the first leading SVD mode in Fig. 11. Consistent with observations, a IOBM warming pattern forces a Matsuno–Gill pattern in the tropospheric temperature, with a warm Kelvin wave propagating into the western Pacific along the equator and Rossby wave–like off-equatorial maxima over the western TIO and Africa. A low-level anticyclone appears on the northern flank of the tropospheric Kelvin wave from the Bay of Bengal to the subtropical WNP. Overall, the AGCM ensemble-mean simulation is able to capture the teleconnection mechanism from the TIO to China.

5. Summary and discussion

We have investigated the impact of tropical IOBM SST anomalies on summer surface air temperature in China through using observations and atmospheric models. When the Indian Ocean SST displays a basinwide

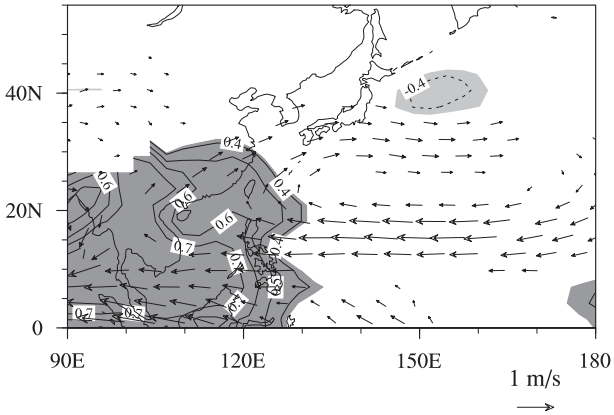

FIG. 10. Correlation of 21-member ensemble-mean simulation lower-level (vertical average from 1000 to 850 hPa) air temperature (contours; shading denotes 90% confidence level) with IOBM index and regression of 21-member ensemble-mean 850-hPa winds (vectors) on IOBM index during 1979–2000. Wind vectors denote 90% confidence level.

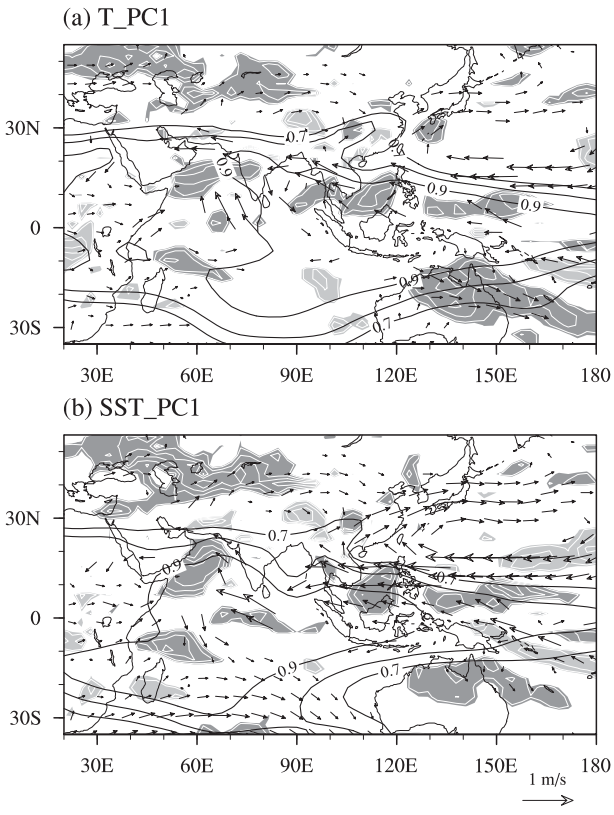

FIG. 11. Correlation with the (a) TS_PC1 (time series of first leading SVD mode of ensemble-mean simulation lower-level air temperature in Fig. 9) and (b) SST_PC1 (the time series of first leading SVD mode of Indian Ocean SST of Fig. 9): 21-member ensemble simulation summer precipitation (white contour interval is 0.1, with $|r| > 0.37$; dark shading denotes positive correlation and 90% confidence level, and light shading denotes negative correlation and 90% confidence level), 850-hPa wind (regression; vector), and tropospheric temperature (vertical average from 850 to 200 hPa; contours). Wind vectors denote 90% confidence level. Analysis is based on the ensemble-mean simulation data from 1979 to 2000.

warming, the summer temperature is above normal in south China and below normal in northeast China. The seesaw pattern of temperature anomalies in China is associated with an anomalous anticyclone circulation over the subtropical northwest Pacific and an anomalous cyclone circulation over Japan, Korea, and northeast China. The anticyclone anomalies and cyclone anomalies, resembling the EAP/PJ teleconnection pattern, can lead to less precipitation and a descending vertical motion in south China and an ascending vertical motion in northeast China. The vertical motion and precipitation anomalies lead to surface air temperature anomalies in south China and northeast China. Moreover, these EAP/PJ pattern–like anticyclone and cyclone anomalies are affected by IOBM SST anomalies through a propagating Kelvin wave. Thus, the meridional dipole circulation anomalies and the Kelvin wave are likely the key processes that convey the remote effect from the TIO to China summer surface air temperature. In this study, we focus the impact of the TIO warming basinwide SST anomalies on surface air temperature. However, the summer surface air temperature anomalies corresponding to TIO cooling basinwide SST anomalies do not reflect the reverse of the TIO warming phase (figure is not shown), suggesting nonlinear impact of IOBM SST anomalies on surface air temperature in China.

Our AGCM hindcast is able to capture the Matsuno–Gill pattern atmospheric response to IOBM SST anomalies, the Kelvin wave over the equatorial western Pacific, and the anomalous anticyclone circulation over subtropical northwest Pacific. But there is no significant anomalous cyclone circulation over the midlatitude of East Asia in the model simulations. Consistent with simulated circulation anomalies, there is a warm tongue over south China in the lower-level troposphere but no significant temperature anomalies over northeast China. The simulation skill is low for midlatitude cyclone anomalies, possibly because of the high atmospheric internal variability there (Lu et al. 2006; Rowell et al. 1995). Nevertheless, the ensemble-mean simulation still captures the temperature meridional dipole structure to some extent.

We also extend the observational analysis to 1951. The results show that the interannual variability of China summer temperature that is impacted by IOBM SST anomalies has experienced a pronounced increase since the late 1970s. The results are consistent with a previous study (Huang et al. 2010) that both the interannual variability of tropical Indian Ocean SST and the teleconnection from the TIO to East Asia have experienced a pronounced increase. Although the interannual variability of IOBM-induced temperature anomalies are larger in the postshift period than the preshift period, the observed summer temperature anomalies in south China have not experienced such a decadal change, which implies that south China temperature variations are also impacted by other factors such as typhoon activity and SST anomalies in the South China Sea (Yan and Huang 2005). However, the interannual variability of northeast China summer temperature has experienced a pronounced increase too.

The present study focuses on the impact of TIO SST anomalies on China surface air temperature on an interannual time scale. However, TIO SSTs have also experienced substantial interdecadal change. Hu (1997) suggests that the tropical Indian Ocean and western Pacific SST persistent warming in recent decades leads

to the surface air temperature change from below normal to above normal in the southern and southwestern parts of China around 1977–79 through modulating the strength and location of the subtropical high. It is interesting that the impact of TIO SST anomalies on summer China surface air temperature on an interdecadal time scale is similar with that induced by IOBM SST anomalies. The question of whether the underlying mechanisms of the impact of IOBM SST anomalies and TIO long-term warming on China surface air temperature are the same needs further study.

Moreover, the SST anomalies in other regions may also contribute to the variability of China surface air temperature. For example, Wu et al. (2010) suggest that SST anomalies in the North Atlantic and the tropical North Pacific can influence northeast China surface air temperature in summer, especially after the late 1970s. Thus, the prediction of summer temperature in China may need comprehensive understanding of the contributions of different oceans and deserves further study.

Acknowledgments. The authors are grateful to Prof. Shang-ping Xie and Prof. Renguang Wu for their helpful discussion and three anonymous reviewers for their useful comments. This work is jointly supported by the National Basic Research Program of China (973 projects) under Grants 2011CB309704 and 2010CB950403, CAS XDA05090402, the National Natural Science Foundation of China (Grants 40890155, U0733002, 40730952, and 40810059005), and Key Laboratory of Global Change and Marine-Atmospheric Chemistry, SOA (GCMAC1006).

REFERENCES

Black, E., M. Blackburn, G. Harrison, B. Hoskins, and J. Methven, 2004: Factors contributing to the summer 2003 European heatwave. *Weather,* **59,** 217–223.

Chowdary, J. S., S.-P. Xie, J.-J. Luo, J. Hafner, S. Behera, Y. Masumoto, and T. Yamagata, 2011: Predictability of northwest Pacific climate during summer and the role of the tropical Indian Ocean. *Climate Dyn.,* **36,** 607–621.

Collins, W. D., and Coauthors, 2006: The Community Climate System Model version 3 (CCSM3). *J. Climate,* **19,** 2122–2143.

Fischer, E. M., S. I. Seneviratne, P. L. Vidale, D. Lüthi, and C. Schär, 2007: Soil moisture–atmosphere interactions during the 2003 European summer heat wave. *J. Climate,* **20,** 5081–5099.

Gill, A. E., 1980: Some simple solutions for heat-induced tropical circulation. *Quart. J. Roy. Meteor. Soc.,* **106,** 447–462.

Haines, A., R. S. Kovats, D. Campbell-Lendrum, and C. Corvalan, 2006: Climate change and human health: Impacts, vulnerability, and mitigation. *Lancet,* **367,** 2101–2109.

Hu, Z.-Z., 1997: Interdecadal variability of summer climate over East Asia and its association with 500 hPa height and global sea surface temperature. *J. Geophys. Res.,* **102,** 19 403–19 412.

——, S. Yang, and R. Wu, 2003: Long-term climate variations in China and global warming signals. *J. Geophys. Res.,* **108,** 4614, doi:10.1029/2003jd003651.

Huang, G., and Z. Yan, 1999: The East Asian summer monsoon circulation anomaly index and its interannual variations. *Chin. Sci. Bull.,* **44,** 1325–1329.

——, K. Hu, and S.-P. Xie, 2010: Strengthening of tropical Indian Ocean teleconnection to the northwest Pacific since the mid-1970s: An atmospheric GCM study. *J. Climate,* **23,** 5294–5304.

Huang, R., and L. Lu, 1989: Numerical simulation of the relationship between the anomaly of subtropical high over East Asia and the convective activities in the western tropical Pacific. *Adv. Atmos. Sci.,* **6,** 202–214.

——, and Y. Wu, 1989: The influence of ENSO on the summer climate change in China and its mechanism. *Adv. Atmos. Sci.,* **6,** 21–32.

——, W. Chen, B. Yang, and R. Zhang, 2004: Recent advances in studies of the interaction between the East Asian winter and summer monsoons and ENSO cycle. *Adv. Atmos. Sci.,* **21,** 407–424.

Kalnay, E., and Coauthors, 1996: The NCEP/NCAR 40-Year Reanalysis Project. *Bull. Amer. Meteor. Soc.,* **77,** 437–471.

Klein, S. A., B. J. Soden, and N.-C. Lau, 1999: Remote sea surface temperature variations during ENSO: Evidence for a tropical atmospheric bridge. *J. Climate,* **12,** 917–932.

Li, S., J. Lu, G. Huang, and K. Hu, 2008: Tropical Indian Ocean Basin warming and East Asian summer monsoon: A multiple AGCM study. *J. Climate,* **21,** 6080–6088.

Lu, R., Y. Li, and B. Dong, 2006: External and internal summer atmospheric variability in the western North Pacific and East Asia. *J. Meteor. Soc. Japan,* **84,** 447–462.

Matsuno, T., 1966: Quasi-geostrophic motions in the equatorial area. *J. Meteor. Soc. Japan,* **44,** 25–43.

McMichael, A. J., R. E. Woodruff, and S. Hales, 2006: Climate change and human health: Present and future risks. *Lancet,* **367,** 859–869.

Nitta, T., 1987: Convective activities in the tropical western Pacific and their impact on the Northern Hemisphere summer circulation. *J. Meteor. Soc. Japan,* **65,** 373–390.

Rayner, N. A., D. E. Parker, E. B. Horton, C. K. Folland, L. V. Alexander, D. P. Rowell, E. C. Kent, and A. Kaplan, 2003: Global analyses of sea surface temperature, sea ice, and night marine air temperature since the late nineteenth century. *J. Geophys. Res.,* **108,** 4407, doi:10.1029/2002JD002670.

Rowell, D. P., C. K. Folland, K. Maskell, and N. M. Ward, 1995: Variability of summer rainfall over tropical North Africa (1906–92): Observations and modelling. *Quart. J. Roy. Meteor. Soc.,* **121,** 669–704.

Saji, N. H., B. N. Goswami, P. N. Vinayachandran, and T. Yamagata, 1999: A dipole mode in the tropical Indian Ocean. *Nature,* **401,** 360–363.

Shi, X., C. Lu, and X. Xu, 2011: Variability and trends of high temperature, high humidity, and sultry weather in the warm season in China during the period 1961–2004. *J. Appl. Meteor. Climatol.,* **50,** 127–143.

Wei, K., and W. Chen, 2009: Climatology and trends of high temperature extremes across China in summer. *Atmos. Oceanic Sci. Lett.,* **2,** 153–158.

Wu, R., S. Yang, S. Liu, L. Sun, Y. Lian, and Z. Gao, 2010: Changes in the relationship between northeast China summer

temperature and ENSO. *J. Geophys. Res.,* **115,** D21107, doi:10.1029/2010D014422.

Xie, P., and P. A. Arkin, 1996: Analyses of global monthly precipitation using gauge observations, satellite estimates, and numerical model predictions. *J. Climate,* **9,** 840–858.

Xie, S.-P., K. Hu, J. Hafner, H. Tokinaga, Y. Du, G. Huang, and T. Sampe, 2009: Indian Ocean capacitor effect on Indo–western Pacific climate during the summer following El Niño. *J. Climate,* **22,** 730–747.

——, Y. Du, G. Huang, X.-T. Zheng, H. Tokinaga, K. Hu, and Q. Liu, 2010: Decadal shift in El Niño influences on Indo–western Pacific and East Asian climate in the 1970s. *J. Climate,* **23,** 3352–3368.

Yan, L.-J., and X.-X. Huang, 2005: On anomalous climatic change of south China temperature in July (in Chinese). *Meteor. Monogr.,* **31,** 64–67.

Yang, J., Q. Liu, S.-P. Xie, Z. Liu, and L. Wu, 2007: Impact of the Indian Ocean SST basin mode on the Asian summer monsoon. *Geophys. Res. Lett.,* **34,** L02708, doi:10.1029/2006GL028571.

Zhai, P., A. Sun, F. Ren, X. Liu, B. Gao, and Q. Zhang, 1999: Changes of climate extremes in China. *Climatic Change,* **42,** 203–218.